Journal of Alloys and Compounds 506 (2010) 434–440

Contents lists available at ScienceDirect

Journal of Alloys and Compounds

journal homepage: www.elsevier.com/locate/jallcom

Size dependence of creep behavior in nanoscale Cu/Co multilayer thin films

X.Y. Zhu[a,b], J.T. Luo[a], G. Chen[a], F. Zeng[a], F. Pan[a,*]

[a] Laboratory of Advanced Materials, Department of Materials Science and Engineering, Tsinghua University, Beijing 100084, People's Republic of China
[b] National Key Lab for Remanufacturing, Academy of Armored Forces Engineering, Beijing 100072, People's Republic of China

ARTICLE INFO

Article history:
Received 7 May 2010
Received in revised form 5 July 2010
Accepted 6 July 2010
Available online 14 July 2010

Keywords:
Cu/Co multilayers
Nanoindentation
Creep
Stress exponent
Interface

ABSTRACT

Cu/Co multilayers with periodicity of 4–40 nm were prepared by electron beam evaporation deposition. Microstructure and room temperature creep behavior were investigated by X-ray diffraction, transmission electron microscopy and nanoindentation test. The results show that superlattice structure forms with decreasing periodicity and coherent interfaces come into being at low periodicity of 4 nm. Size dependence of the creep behavior is observed and power-law creep parameters including stress exponent and size sensitivity index are calculated by dimension analysis. A dislocation model for predicting the steady-state deformation of multilayers with semi-coherent interfaces is presented. Nanoscale effects are explained by dislocation generation and annihilation mechanisms involving single dislocations slip in confined layers and dislocations climb at the interfaces, respectively. Model predictions agree well with experimental observation.

1. Introduction

The influence of scale on the mechanical properties of multilayers has long been of interest since large hardness enhancement compared with monolithic coatings of the constituent materials has been found [1,2]. Through studying the evolution of film strength as a function of periodicity, the length-scale-dependent strengthening mechanisms have been well documented [3]. However, scale dependence of rate-controlling deformation mechanisms in multilayers has less been investigated, even though some researchers have already focused their eyes on room temperature creep phenomena in thin films due to the necessary to practical applications [4–6]. Recently, size dependence of power-law creep observed in nanocrystalline has received much attention and several models have been proposed [7–9]. It is believed that, different from coarse-gained materials, dislocations in nanocrystalline are mainly located at high-angle boundaries, and thus both the rates of dislocations generation and dislocations recovery are enhanced. As a result, explicit size dependence of steady-state deformation appears. Plastic deformation in nanoscale multilayers is expected far more complex than that in nanocrystalline because interfaces which play a key role in the plastic deformation have very different structures in different types of systems. In fact, discrepant size-dependent creep behavior has already been reported in several multilayer systems [10–12]. It is obvious that the rate-controlling deformation mechanisms in multilayers is still unclear and is open for investigation.

With the development of depth-sensing indentation technique, it is accepted that nanoindentation test provides a simplest and most direct way to probe the mechanical properties, including creep, of thin films [13,14]. As one of the widely used method, constant-load indentation (CLI) experiment records the hardness value with decreasing indentation strain rate during the load-holding segment, so the tabulation of several hardness-indentation strain rate pairs can be applied to analyze the creep process [15–18]. Although nanoindentation creep behavior is considerably more complex than that measured by conventional uniaxial tensile tests, creep parameters such as stress exponent are in good agreement with those values obtained by conventional methods [19–22].

Cu/Co is one of the most studied multilayer systems for it is an ideal candidate for magnetic sensors and electronic switching elements due to its giant magnetoresistance (GMR) [23]. In the present work, we investigate room temperature indentation creep in Cu/Co multilayers using the CLI method. Creep parameters including stress exponent and size sensitivity index are calculated by dimensional analysis. A dislocation model based on dislocations generation and annihilation at interfaces is developed to account for the nanoscale effects.

2. Experimental details

Cu/Co multilayers were deposited onto Si(1 0 0) wafers at room temperature by alternate electron beam evaporation deposition of Cu and Co using an ultra high vacuum (UHV) chamber. The base vacuum of the chamber was 5×10^{-7} Pa. Prior to the deposition of Cu/Co multilayers, a 10-nm-thick Ti layer was deposited to improve the cohesion between the film and the substrate. The deposition rates were 0.5 Å/s for both Cu and Co. The nominal thickness of individual Cu and Co layers was

* Corresponding author. Tel.: +86 10 62772907; fax: +86 10 62771160.
E-mail address: panf@mail.tsinghua.edu.cn (F. Pan).

0925-8388/$ – see front matter © 2010 Elsevier B.V. All rights reserved.
doi:10.1016/j.jallcom.2010.07.024

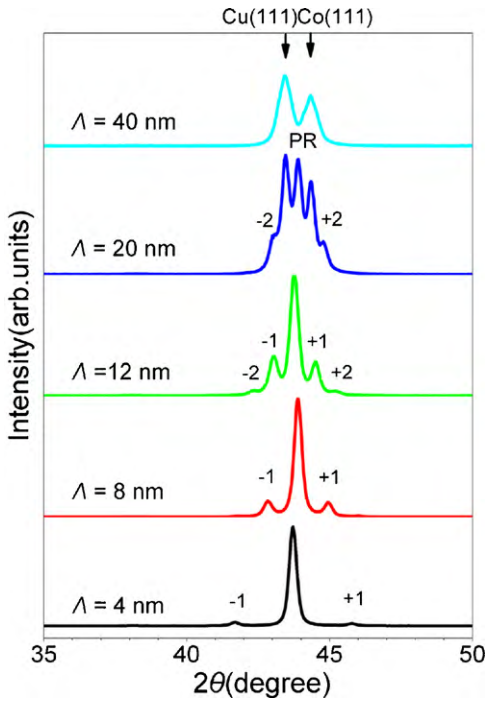

Fig. 1. The XRD patterns for all the Cu/Co multilayers.

monitored by an in situ quartz oscillator and all the multilayers were controlled to have equivalent Cu and Co layers but different periodicity ranging from 4 nm to 40 nm. The total thickness of films was approximately 600 nm.

X-ray diffraction (XRD) experiment was adopted to investigate the microstructure using Rigaku D/max-RB X-ray diffractometer with Cu Kα radiation. Transmission electron microscopy (TEM) with selected-area diffraction (SAD) was performed using a JEM2010 high-resolution electron microscopy (HRTEM) with 200 kV accelerating voltages. The mechanical properties of the multilayers, as well as the Cu and Co monolithic layers, were investigated by a Nano Indenter XP (MTS Systems Corp.) with a displacement resolution of less than 0.01 nm and loading resolution of 50 nN. A Berkovich indenter, a three-sided pyramid with the same area-to-depth function as that of a Vickers indenter, was used in all the tests. The hardness of the multilayers was measured by a continuous-stiffness measurement (CSM) technique with a load strain rate of 0.05 s^{-1}. Indentation creep process was tested at room temperature by a constant-load indentation (CLI) method. A series of indents was made on each sample at an inter-indent spacing of 50 μm, and the mean values of the creep data were then calculated in order to minimize the deviation of results after the extreme values were rejected.

3. Results and discussion

3.1. Microstructure

X-ray spectra recorded with standard θ–2θ reflection geometry of Cu/Co multilayers is shown in Fig. 1. For the multilayer with Λ = 40 nm, only two main Bragg reflections located at 43.4° and 44.3° are observed, indicating strong ⟨1 1 1⟩ texture along the film normal. When the periodicity decreases to 20 nm, another principal reflection located at 43.9° appears, which is not the characteristic of Cu or Co plane spacing but intermediate between the spacing characteristics of Cu (1 1 1) and Co (1 1 1). We presume that this principle peak is the reflection of the epitaxial Co/Cu (1 1 1) planes. With the decreasing periodicity, the reflections of Cu (1 1 1) and Co (1 1 1) disappear and only the principal reflection can be observed. Moreover, the principal reflection is flanked symmetrically by some additional satellite peaks and their position agrees well with the periodicity predicted by the deposition rate calibrations. The XRD spectra indicates that superlattice structure forms with the decreasing periodicity as 2.0% lattice mismatch within close-packed planes between Cu (1 1 1) and Co (1 1 1) is accommodated and manifested by the single Bragg reflection at

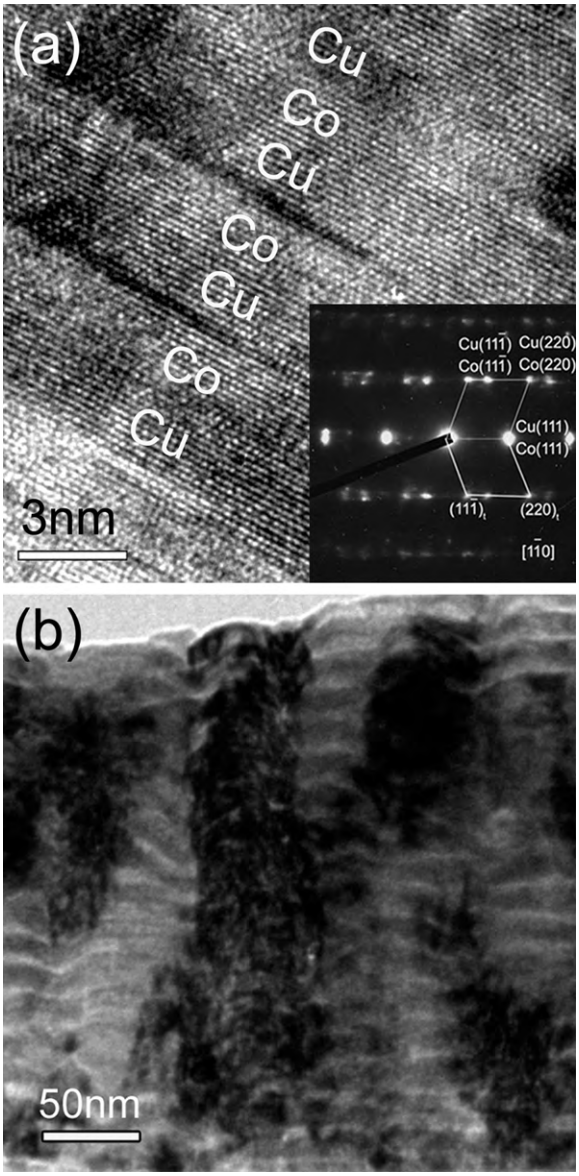

Fig. 2. (a) The cross-section HRTEM image and the corresponding SAD pattern confirm coherent interfaces in the multilayer with Λ = 4 nm. (b) The transmission electron micrograph taken in bright field of the multilayer with Λ = 20 nm shows the layered structure with columnar grains.

~43.9°.On the other hand, it is well known that full coherent interfaces can form only below a critical layer thickness h_c [24]. When layer thickness is above this critical value, a square grid of misfit dislocations between semi-coherent interfaces will form to relax coherency stresses. Experimental observations in Cu/Co superlattices have revealed that coherent interfaces remain for layers up to 4 nm [25,26], thus, we assume that full coherent interfaces will come into being at Λ = 4 nm in Cu/Co multilayers.

Cross-section transmission electron micrographs provide a more intuitive view of the interfacial structure at small periodicity. Fig. 2(a) shows the high-resolution electron micrograph of the multilayer with Λ = 4 nm. Layered structure is still maintained at Λ = 4 nm and coherent interfaces between Cu and Co layers have been observed. Moreover, the corresponding SAD pattern with [1 $\bar{1}$ 0] zone axis, as inserted in Fig. 2(a), also confirms the coherence with the orientation relationship of $(1\,1\,1)_{Cu}//(1\,1\,1)_{Co}$. Apart from this, a twining structure with (1 1 1) twin planes parallel to the layer interfaces is implied. Fig. 2(b) shows the bright field image

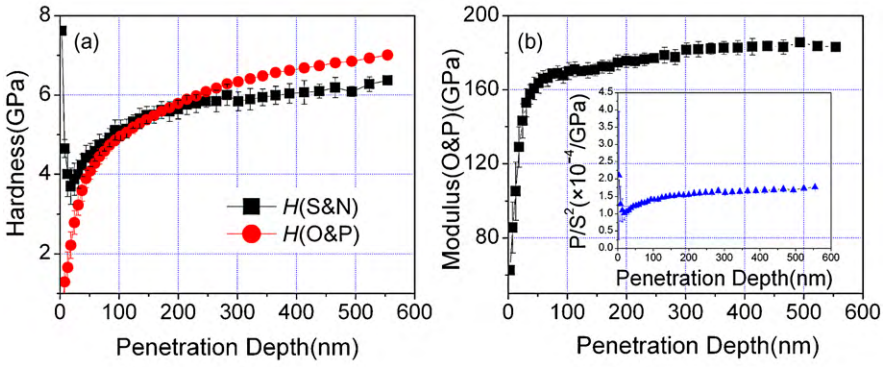

Fig. 3. (a) Hardness values of the Cu/Co multilayer with $\Lambda = 4$ nm determined by Oliver and Pharr method and Saha &Nix method are plotted as functions of penetration depth, respectively. (b) Modulus of the Cu/Co multilayer with $\Lambda = 4$ nm determined by Oliver and Pharr method is plotted as a function of penetration depth. The plateau region at the penetration depth of 100–200 nm indicates the intrinsic modulus value of 170 ± 4 GPa. The inset shows P/S^2 as a function of the penetration depth. P/S^2 keeps constant at penetration depth exceeding 100 nm, demonstrating that the film/substrate system is elastically homogenous.

of the multilayer with $\Lambda = 20$ nm, from which we can see that the multilayer exhibits layered structure with columnar growth morphology. Most of the grains extend across the full thickness of the deposited films and the average width of the columnar grains is about 60 nm. The average in-plane grain size of the other samples is also examined. The results reveal that the in-plane grain size decreases with decreasing periodicity and it was around 20 nm at $\Lambda = 4$ nm, much larger than the periodicity.

3.2. Nanoindentation creep

As the total film thickness of the Cu/Co multilayers is approximately 600 nm, before the room temperature creep properties is discussed, the effects of the substrate on the determination of film mechanical properties by nanoindentation is considered at first. The nanoindentation data were measured continuously during the loading of the indenter by the CSM method and then analyzed by the Oliver and Pharr method [27]. The hardness and modulus [denoted as H(O&P) and E(O&P)] with penetration depth for the multilayer with $\Lambda = 4$ nm are presented in Fig. 3(a) and (b). It is found that the hardness values increase continuously with the penetration depth and no distinct plateau is observed. Whereas the modulus values rise slightly after exhibiting a plateaus value about 172 ± 2 GPa in the range of 100–200 nm, indicating a modulus value of 172 GPa. Similar variations in other Cu/Co multilayers with different periodicity are observed and the plateaus values that exist in the modulus curves do not vary significantly with the periodicity. For thin films, the variations in H(O&P) and E(O&P) are usually considered to arise from either pile-up or substrate effects. Since Cu/Co multilayers deposited on Si(1 0 0) water can be regarded as soft film on hard substrate system, the plastic deformation occurs only in the films when the penetration depth is less than the film thickness. Furthermore, if the plateaus value in the modulus curve is the intrinsic modulus of the multilayer, as it is as the same as that of Si(1 0 0) (172 GPa) [28], the film and substrate system can be regarded as elastic homogeneous. Joslin and Oliver have proposed that the parameter $P/S^2 = \pi H/4\beta^2 E_r^2$ can be used to discuss the nanoindentation properties of a film/substrate system, where P is the load on the sample, S is contact stiffness, β is a constant that depends on the geometry of the indenter and E_r is reduced modulus, because hardness and reduced modulus are usually constant with penetration depth for homogeneous materials, thus, P/S^2 is also constant with penetration depth [29]. The parameter P/S^2 is plotted as a function of penetration depth in the insert in Fig. 3(b). It keeps a constant value about 1.5×10^{-4} GPa after 100 nm, demonstrating that the film/substrate system is elastically matched. The initial variation in parameter P/S^2 at shallow depth originates from either indentation size effects or surface effects. Therefore, substrate effects on Cu/Co multilayers mechanical properties can be excluded and the increase in hardness and modulus with penetration depth is ascribed to the effect of pile-up. In order to avoid pile-up effect, we calculate the hardness value using the equation $H = 4\beta^2 P E_r^2/\pi S^2$ developed by Saha and Nix [28]. As the system is elastically homogeneous, E_r is deduced from the equation $1/E_r = (1 - \nu_i^2)/E_i + (1 - \nu_f^2)/E_f$ [27], where i and f denote indenter and film, respectively. As the hardness is determined by measuring the parameter P/S^2, reduced modulus E_r, and the contact area A_c is not included directly, the errors associated with underestimation of the contact area A_c are eliminated by this method. Hardness calculated by this method [denoted as H(S&N)] is plotted as a function of penetration depth in Fig. 3(a). Comparing H(S&N) with H(O&P), we find that they are consistent well in the range of 100–200 nm whereas a apparent deviation can be observed after that. H(S&N) gradually approaches a constant value of 5.88 GPa in the range of 200–300 nm while H(O&P) keeps increasing with increasing penetration depth. It indicates that the errors associated with pile-up are insignificant until the penetration depth exceeds 200 nm.

To avoid the effects of pile-up and surface roughness on the nanoindentation hardness values, we performed the room temperature creep tests by loading all the samples to a predetermined penetration depth of 100 nm at a constant-load strain rate of $0.05\ s^{-1}$ and then holding the load constant for 10 min to record the variations in indentation depth and hardness values continuously. After that, all the samples were unloaded to 10% of the maximum load and then the load was held constant for a further 2 min to measure the thermal drift in order to adjust nanoindentation data that recorded in the creep process. Finally the indenter was withdrawn from the samples to zero load. A typical load-unload schedule is shown in Fig. 4.

The relations between indentation displacement and holding time for all the samples are plotted in Fig. 5(a). The data show that all the creep process presents same tendency, that is, an initial sharp rise in indentation displacement followed by a region with a smaller rate of increase. Usually, the initial stage corresponds to “transient creep” and the secondary stage corresponds to “steady-state creep”. Meanwhile, size dependence of creep behavior is observed as the total creep depth augments with the increasing periodicity. Since all the creep tests are performed at same indentation depth, the load and stress applied on every sample vary according to their intrinsic hardness. Hence the influence of load and/or stress is needed to be considered as the variation in the creep displacement is discussed. We regard the hardness values at the end of the holding time as the apparent average stress $\bar{\sigma}$ in the steady-state creep stage and present them, together with holding load

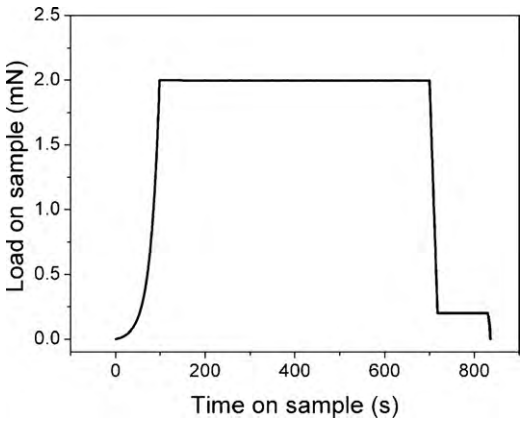

Fig. 4. The load–unload sequence for a constant-load indentation creep experiment.

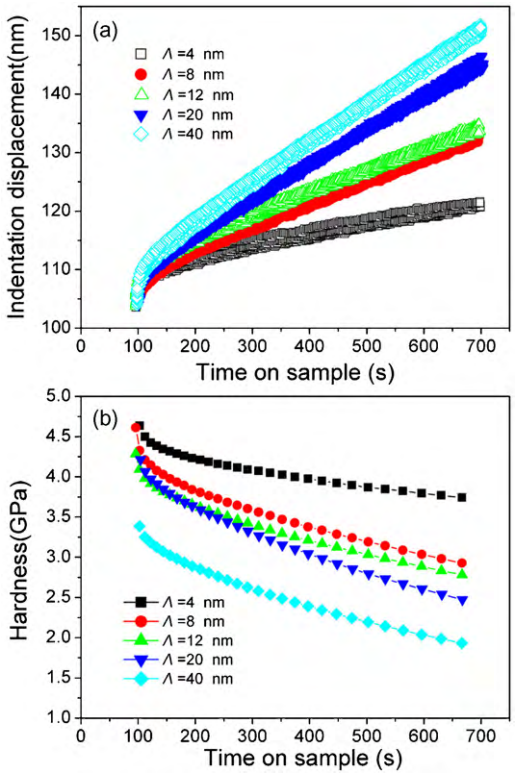

Fig. 5. (a) Variations in indentation displacement and (b) variations in hardness as functions of time of all the samples.

values P_{max} and total creep displacement μ, in Table 1. Clearly, the decrease in creep displacement with decreasing periodicity cannot be caused by different holding load or stress, because the multilayer with $\Lambda = 4$ nm exhibits smallest creep displacement of 16.11 nm under highest holding load of 2.02 mN and average stress level of 3.74 GPa while the multilayer with $\Lambda = 40$ nm exhibits largest creep displacement of 41.47 nm under lowest holding load of 1.55 mN and average stress level of 1.93 GPa. Additionally, this phenomenon implies that diffusion or grain boundaries sliding cannot be the dominant creep mechanism because one of the characteristics of diffusion creep or grain boundaries sliding is that the creep rate increases with decreasing grain size according to $\dot{\varepsilon} \propto 1/d^2$ or $1/d^3$ [30]. If the creep is controlled by diffusion or grain boundaries sliding, the creep displacement of all the samples should increase with decreasing periodicity. Thereby, we preliminarily conclude that the inherent mechanism for indentation creep is controlled by dislocation movement.

Table 1
Holding load values P_{max}, apparent average stress $\bar{\sigma}$ and creep displacement μ of all the multilayers.

Λ (nm)	P_{max} (mN)	$\bar{\sigma}$ (GPa)	μ (nm)
4	2.02	3.74	16.11
8	1.81	2.93	28.69
12	1.84	2.78	29.74
20	1.86	2.47	37.64
40	1.55	1.93	41.47

Although dislocation glide-climb mechanism is traditionally thought to dominate the creep process only as homologous temperature above $0.5T_m$, room temperature creep process dominated by dislocation climb have been observed in metallic thin films [4,5] and nanocrystalline materials [31]. It was explained that the highly dense dislocations in the indent core or grain boundaries can provide effective diffusion paths, thus, dislocation climb can operate very effectively even at room temperature. In fact, dislocation climb is more likely to occur in multilayers because interfaces can act as sources to emit and absorb the vacancies and interstitials and then enhance their recombination. In face, Wang et al. have investigated room temperature dislocation climb in metallic interface of Cu/Nb multilayer system using atomistic simulation [32]. It reveals that a mixed dislocation in the interfaces acts as a sink for absorbing vacancies accompanied with a counter diffusion of Cu atoms to the dislocation core. Consequently, a patch of extra Cu(1 1 1) forms at the end of the half plane of Nb(1 1 0). Through climb, the out-of plane component of the mixed dislocation dissociates into two parts. Then they are separated through climb in the interface due to the associated large decrease in the line energy. One climbs through absorption of vacancies, but the other one through emission of vacancies, both associated with a counter diffusion of Cu atoms in the interface. Thus, these two parts can spread in the interface widely and when two dislocations of opposite sign encounter, they will dissolve and lead to dislocation annihilation. More details about the room temperature climb process can be found in Ref. [32]. Similar climb process is expected to occur in Cu/Co multilayers.

In order to further clarify the creep mechanism, we use the constitutive equation to analyze the creep process. Some investigators have demonstrated that indentation creep curves could be analyzed by applying steady-state creep equation [33,34]:

$$\dot{\varepsilon} = A\sigma^n \tag{1}$$

where A is a constant related with temperature, n is stress exponent. When the size dependence of power-law creep is concerned, the steady-state creep strain rate can be indicated by a modified grain size-dependent form

$$\dot{\varepsilon} = A\left(\frac{\Lambda}{2}\right)^p \sigma^n \tag{2}$$

where $\Lambda/2$ is layer thickness and p is size sensitivity index. For indentation creep with a self-similar indenter, the creep strain rate $\dot{\varepsilon}$ is defined as $\dot{\varepsilon} = C/\sqrt{A_c} \cdot (dh/dt)$ and indentation contact stress σ is defined as $\sigma = P/A_c$, where h is indentation displacement, t is time and C is a constant dependent on indenter shape. Using the dimensional analysis suggested by Sargent and Ashby [35], we get the following relation from Eq. (2):

$$H(t) = \frac{1}{[A_1(\Lambda/2)^p]^{1/n} t^{1/n}} \tag{3}$$

$$\ln\ H(t) = -\frac{1}{n}\ln t - p\ln(\Lambda/2)^{1/n} + A_2 \tag{4}$$

where A_1 and A_2 are constants related with indenter shape and temperature. For every sample with specific periodicity, as the

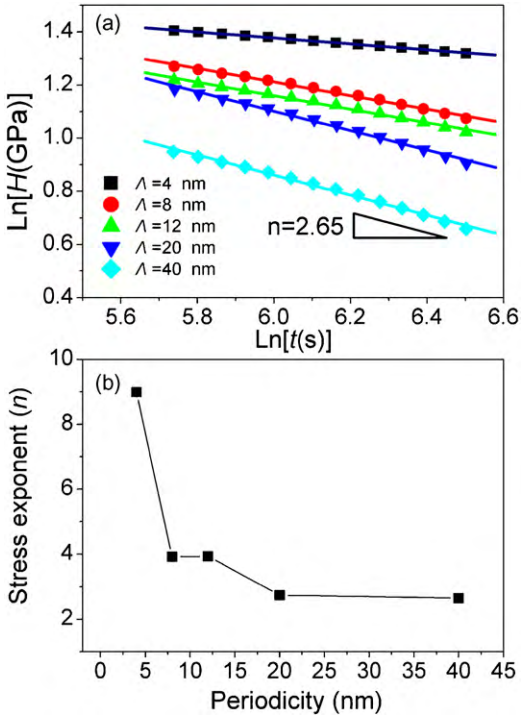

Fig. 6. (a) $\ln H$–$\ln t$ plots for all the multilayers. The slope of these lines will be $(-1/n)$ from which the stress exponent, n, is determined. (b) The stress exponent show a slight dependence on periodicity at $\Lambda \geq 8$ nm while an apparent rise is observed at $\Lambda = 4$ nm.

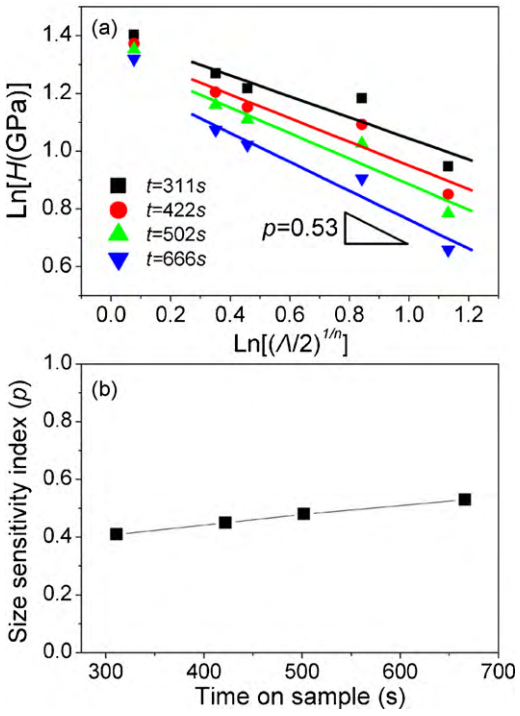

Fig. 7. (a)$\ln H$–$\ln(\Lambda/2)^{1/n}$ plots for all the multilayers. The slope of these lines will be $(-p)$ from which the size sensitivity index, p, is determined. (b) Size sensitivity index of Cu/Co multilayers calculated at different time approaches a steady value around 0.5 with extending holding time.

creep test was performed at room temperature, n-values can be calculated by the gradient of a plot of $\ln H$ against $\ln t$. Then, inserting such n into Eq. (4), we can obtain p-values by the gradient of a plot of $\ln H$ against $\ln(\Lambda/2)^{1/n}$. Variations in hardness of all the samples with holding time are plotted in Fig. 5(b). Hardness decreases with holding time because of the increase in indentation displacement. Moreover, it drops dramatically in the initial creep stage compared with the secondary creep stage, which is due to the mechanical transient effects and inertia effects that dominate the transient creep [34]. Hence, we only take the hardness values obtained after 300 s into account when discussing stress exponent and size sensitivity index. $\ln H$ as a function of $\ln t$ is plotted in Fig. 6(a) and obvious linear relationships are observed in all the samples. The n-values extracted from Fig. 6(a) vary from 2.65 to 8.99, as plotted in Fig. 6(b), further confirming an inherent creep mechanism controlled by dislocation glide-climb. Furthermore, we notice that the stress exponent shows a slight dependence on periodicity at $\Lambda \geq 8$ nm, giving an average value of 3.31. Later, a sharp rise to 8.99 occurs at $\Lambda = 4$ nm. Similar variation in stress exponent has also been observed in our previous research on Cu/Ni system [11]. The stress exponent in Cu/Ni system varies around an average value of 2.74 at $\Lambda \geq 14$ nm and a significantly increase to 6.78 at $\Lambda = 10.5$ nm. In order to calculate the size sensitivity index, we present $\ln H$ that obtained at different time intervals of 311 s, 422 s, 502 s and 666 s respectively as functions of $\ln(\Lambda/2)^{1/n}$, as shown in Fig. 7(a). It can be seen that at $\Lambda \geq 8$ nm, similar linear relationships are observed at different time and the p-values calculated by the gradient approaches a steady value around 0.5 with extending holding time, as plotted in Fig. 7(b). However, at $\Lambda = 4$ nm the linear relationships trend to break up and a higher p-value is expected.

3.3. A dislocation model for steady-state deformation

As the Cu/Co multilayers have columnar grain structure, two kinds of characteristic length scale, layer thickness $\Lambda/2$, and in-plane grain size, d, are needed to be considered when the deformation mechanism is concerned. Verdier et al. have proposed a deformation mechanism map which takes the role of $\Lambda/2$ and d into account and have found that in the region where the in-plane grain size is much larger than the layer thickness, the layer thickness acts as the dominant length scale [36]. Moreover, it is generally accepted that the dominate deformation mechanism operating in nanoscale multilayers is single dislocations slip in confined layers at the few to a few tens of nanometers length scale because dislocation pile-ups can not form in such small length scale [3]. Therefore, for the Cu/Co multilayers with periodicity of 4–40 nm, the steady-state creep process is induced by the glide of dislocations in confined layers and mixed dislocations are deposited at the intersection of {1 1 1} glide planes and the layer interfaces during deformation [37,38]. That is to say, $\mathrm{d}\rho^{+}$ dislocations will generate at the interfaces during a shear strain interval $\mathrm{d}\gamma$. The applied shear stress τ required to propagate a glide loop of Burgers vector b confined to one layer can be calculated by the equation

$$\tau = \frac{\mu b}{8\pi h'}\left(\frac{4-\upsilon}{1-\upsilon}\right)\left[\ln\frac{\alpha h'}{b}\right], \quad (5)$$

where μ is the shear modulus, h' is the layer thickness measured parallel to the glide plane and α represents the core cutoff parameter [3]. We find that single dislocations will propagate successively in Cu layers while Co layers continue to deform elastically because of the higher value of the shear modulus in Co layers. For example, for the multilayer with $\Lambda = 20$ nm, as $\mu_{Cu} = 45$ GPa and $\mu_{Co} = 71$ GPa, taking $\alpha \approx 0.3$ for an estimation [11], we find that $\tau_{Cu} \approx 0.60$ GPa while $\tau_{Co} \approx 0.91$ GPa. Multiplied by the Taylor factor of 3.1, the stress that needed for the initial glide of "hairpin" dislocation loops confined in Cu layers and Co layers are calculated to be 1.86 GPa and 2.82 GPa, respectively. It means that under the average stress of 2.47 GPa in the steady-state creep process, the single dislocations in the Cu layers will start to slip while the Co layers keep deforming elastically. This deformation process is schematically shown in

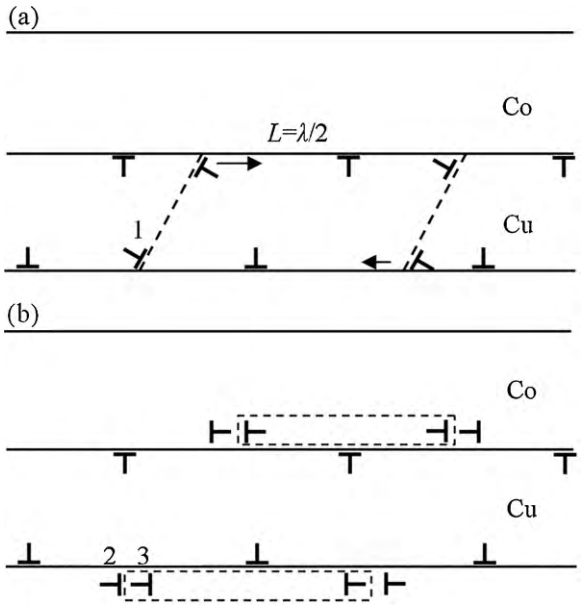

Fig. 8. Schematic representation of dislocations generation by single dislocations slip in confined layers and dislocations annihilation by climb along the interfaces. (a) Gild dislocations propagate successively in confined Cu layers while Co layers continue to deform elastically (dashed line represents slip plane). Mixed dislocations (e.g. dislocation labeled 1) are deposited at the interfaces and finally arrive at the equilibrium position at $L = \lambda/2$. (b) Mixed dislocations dissociate into interfacial dislocations (such as those labeled 2 and 3), and two interfacial dislocations of opposite sign configurate a dislocation dipole (encircled in b). Atomic diffusion along the interfaces leads to the dissolution of the dislocation dipoles.

Fig. 8(a). The mixed interface dislocations will finally arrive at equilibrium position at $L = \lambda/2$ due to the affects of the edge-type misfit dislocations, where λ is the equilibrium spacing of misfit dislocations [24,39]. Sevillano et al. have proposed specific reasons for the relation of dislocation generation when the grain size is below a characteristic length and size effects are expected [40]

$$\frac{d\rho^+}{d\gamma} \propto \left(\frac{1}{d}\right)^{2/3} \tag{6}$$

where d is the sample dimension and can be regarded as $\Lambda/2$ in multilayers. On the other hand, using atomic simulations on Cu/Nb multilayers, Wang et al. have shown that reactions between interfacial dislocations assisted by climb could lead to annihilation of dislocation content [32,41]. As shown in Fig. 8, the mixed dislocations (e.g. the dislocation labeled 1 in Fig. 8(a)) at interfaces can dissociate into interfacial dislocations [e.g. the dislocations labeled 2 and 3 in Fig. 8(b)] having out-of-plane component of Burgers vector through the transport of vacancies and Cu atoms within the interface (the in-plane components of Burgers vector are not shown in the figure). As a consequence, dislocations can widely spread in the interfaces, which will lead to dislocations annihilation when two dislocations of opposite sign are dissolved. In order to estimate the rate at which dislocations are recovered at interfaces, we make the simplifying assumptions that each interfacial dislocation dissociated from mixed dislocations has a neighbor of the same sign (coming from the same mixed dislocation) and a neighbor of opposing sign (coming from the neighboring mixed dislocation). Two interface dislocations with opposite sign configurate a dislocation dipoles, as indicated by the dashed rectangle. Thermally activated dislocations annihilation is assumed to be controlled by time-dependent dissolution of interfacial dislocation dipoles by climb at the rate

$$\frac{d\rho^-}{dt} = f_c \cdot \rho_{dip} \tag{7}$$

where f_c is the frequency of dissolution of dislocation dipoles by climb and ρ_{dip} is the density of dipolar dislocations at interfaces. This density equals a fraction f_{dip} of total ρ, and f_c is expressed as $f_c = v_{c,b}/s_b$, where $v_{c,b}$ is the average climb velocity and s_b is the distance between the dipole components. As indicated in Fig. 8, $s_b = \lambda$ could be assumed for multilayers with semi-coherent interfaces. Using MD simulations, Wang et al. have found that the dislocation climb observed in Cu/Nb multilayers involves only diffusion in the interfacial Cu planes and the diffusion of Nb atoms in the interfaces or of either Cu or Nb in the bulk crystals is negligible [32]. It is ascribed to a huge difference in the formation energies of vacancies in Cu and Nb crystals compared to vacancy formation within the interfaces and the decrease in energies as Nb vacancy is exchanged with an interfacial Cu atom thereby creating a Cu vacancy. Furthermore, they point out that the rate of climb depends on the vacancy concentration and vacancy diffusivity in the interface and calculate the climb velocity in Cu/Nb multilayers at the room temperature is a constant around 0.5 m/s. Similarly, only the diffusion in the interfaces needed to be taken into account as the climb velocity $v_{c,b}$ in the Cu/Co multilayers is considered. Moreover, it can be also estimated as a constant although both the diffusion of Cu atoms and Co atoms in the interfacial planes may be involved in the dislocation dissolution. Thus, the dislocation annihilation is expressed as:

$$\frac{d\rho^-}{dt} = f_{\text{dip}} \cdot \frac{v_{c,b}}{s_b} \cdot \rho \tag{8}$$

For the steady-state creep process, the average dislocation density ρ remains constant with straining due to balance between dislocations generation and annihilation, expressed as $d\rho^+ = d\rho^-$. Then, dislocation generation $d\rho^+/d\gamma$ is rewritten as:

$$\frac{d\rho^+}{d\gamma} = \frac{d\rho^-}{d\gamma} = \frac{1}{\dot{\gamma}}\frac{d\rho^-}{dt} \tag{9}$$

Inserting Eqs. (6) and (8) into (9), we obtain the relation

$$\dot{\gamma} = \frac{d\rho^-/dt}{d\rho^+/d\gamma} \propto \left(\frac{\Lambda}{2}\right)^{2/3} \frac{v_{c,b}}{s_b}\rho \tag{10}$$

For fcc metals deformed at room temperature, the applied resolved shear stress can be estimated using Taylor equation $\tau = \alpha\mu b\sqrt{\rho}$, where α is a constant. Therefore, the steady-state relation between normal strain rate $\dot{\varepsilon} = \dot{\gamma}/M$ and normal stress $\sigma = \tau/M$ (M is Taylor factor) is established as:

$$\dot{\varepsilon} \propto \left(\frac{\Lambda}{2}\right)^{2/3} \frac{v_{c,b}}{s_b}\sigma^2 \tag{11}$$

We can see that dislocation spacing s_b plays a key role in the steady-state creep. Larger s_b leads to a lower rate of recovery and a lower strain rate. That is to say, it results in strengthening. In semi-coherent interfaces, s_b approximately equals to the equilibrium spacing of misfit dislocations $s_b = \lambda = b/\delta$, where δ is the mismatch strain between layers. For $b_{Cu} = 0.25$ nm and $\delta = 2(a^{Cu} - a^{Co})/(a^{Cu} + a^{Co}) \approx 2\%$, $s_b = 12.5$ nm. Therefore, Eq. (11) yields a relation $\dot{\varepsilon} \propto (\Lambda/2)^{2/3}\sigma^2$. It predicts that for multilayers with semi-coherent interfaces, the steady-state creep process will give a p-value of 0.67 and an n-value of 2.

Comparing the model predicted values with the experimental data, we find that they are consistent well at $\Lambda \geq 8$ nm although the predicted values are slightly smaller than the experimental data. This discrepancy may be due to the contribution of grain boundaries which is not considered in the present model. For Cu/Co multilayers with columnar grain structure, grain boundaries can also provide effective diffusion paths for the creep climb, which may have modified the stress dependence of the creep rate. While the present model gives good predictions for the steady-state deformation, at $\Lambda = 4$ nm, the experimental value of stress exponent sharply increases to 8.99, which is much higher than

the predicted value. This problem may arise from two aspects. First, the estimation $s_b = \lambda = b/\delta$ is achieved only in semi-coherent interfaces. Thus, at $\Lambda = 4$ nm where full coherent interfaces have formed, the relation $\dot{\varepsilon} \propto (\Lambda/2)^{2/3}\sigma^2$ is invalid. The increase in the stress exponent occurred at $\Lambda = 14$ nm in Cu/Ni system can be also explained by this reason because the coherency is observed to lose at critical layer thickness about 5 nm in that system [24]. Secondly, although the creep process is still controlled by dislocation glide-climb mechanism at $\Lambda = 4$ nm as indicated by the stress exponent, the deformation model has already changed from single dislocation slip in confined layers to crossing of dislocations across interfaces at a couple nanometers [3]. Thus, we hypothesize that the dislocation model involving single dislocations slip in confined layers and dislocations climb at the interfaces is no longer applicable at $\Lambda = 4$ nm. Furthermore, as coherent interfaces form at $\Lambda = 4$ nm, the alternating compression-to-tension in-plane coherent stresses will block the cross of dislocations across interfaces effectively, which leads to the increase in the stress exponent.

4. Conclusions

In summary, microstructure and room temperature indentation creep of Cu/Co multilayers with periodicity of 4–40 nm were investigated. The results show that superlattice structure forms with decreasing periodicity and coherent interfaces come into being as periodicity down to 4 nm. Size dependence of the power-law creep is observed and the steady-state relation between strain rate and stress is discussed by dimension analysis. A dislocation model is proposed to predict the stress exponent and size sensitivity index during the steady-state deformation in multilayers with semi-coherent interfaces. The model involves single dislocations slip in confined layers and dislocation climb mechanism at the interfaces, and can well describe the experimental observations.

Acknowledgements

The authors are grateful for financial supports from the National Natural Science Foundation of China (Grant Nos. 50871060 and 50772055), National High-tech Project of China (Grant No. 2009AA034001) and National Basic Research Program of China (Grant No. 2010CB832905).

References

[1] M. Stueber, H. Holleck, H. Leiste, K. Seemann, S. Ulrich, C. Ziebert, J. Alloys Compd. 483 (2009) 321–333.
[2] S.P. Wen, R.L. Zong, F. Zeng, Y. Gao, F. Pan, Acta Mater. 55 (2007) 345–351.
[3] A. Misra, J.P. Hirth, R.G. Hoagland, Acta Mater. 53 (2005) 4817–4824.
[4] Z.S. Ma, S.G. Long, Y.C. Zhou, Y. Pan, Scripta Mater. 59 (2008) 195–198.
[5] Z.H. Cao, P.Y. Li, X.K. Meng, Mater. Sci. Eng. A 516 (2009) 253–258.
[6] J. Sarkar, S. Saimoto, B. Mathew, P.S. Gilman, J. Alloys Compd. 479 (2009) 719–725.
[7] W. Blum, X.H. Zeng, Acta Mater. 57 (2009) 1966–1974.
[8] L. Lu, M. Dao, T. Zhu, J. Li, Scripta Mater. 60 (2009) 1062–1066.
[9] M. Huang, P.E.J. Rivera-Diaz-del-Castillo, O. Bouaziz, S. van der Zwaag, Mater. Sci. Technol. Lond. 25 (2009) 833–839.
[10] B.C. Kang, H.Y. Kim, O.Y. Kwon, S.H. Hong, Scripta Mater. 57 (2007) 703–706.
[11] X.Y. Zhu, X.J. Liu, R.L. Zong, F. Zeng, F. Pan, Mater. Sci. Eng. A 527 (2010) 1243–1248.
[12] S.P. Wen, R.L. Zong, F. Zeng, Y. Gao, F. Pan, J. Mater. Res. 22 (2007) 3423–3431.
[13] Y.J. Huang, Y.L. Chiu, J. Shen, J.J.J. Chen, J.F. Sun, J. Alloys Compd. 479 (2009) 121–128.
[14] S.R. Jian, J.S.C. Jang, J. Alloys Compd. 482 (2009) 498–501.
[15] X.Y. Zhu, X.J. Liu, F. Zeng, F. Pan, Mater. Lett. 64 (2010) 53–56.
[16] N. Janakiraman, F. Aldinger, J. Am. Ceram. Soc. 93 (2010) 821–829.
[17] F. Wang, K.W. Xu, Mater. Lett. 58 (2004) 2345–2349.
[18] S. Nowak, P. Ochin, A. Pasko, O. Maciejak, P. Aubert, Y. Champion, J. Alloys Compd. 483 (2009) 139–142.
[19] Y.C. Liu, J.W.R. Teo, S.K. Tung, K.H. Lam, J. Alloys Compd. 448 (2008) 340–343.
[20] H.M. Liu, Y.G. Chen, Y.B. Tang, S.H. Wei, G. Niu, J. Alloys Compd. 440 (2007) 122–126.
[21] R. Mahmudi, A.R. Geranmayeh, A. Rezaee-Bazzaz, J. Alloys Compd. 427 (2007) 124–129.
[22] R. Mahmudi, A. Rezaee-Bazzaz, H.R. Banaie-Fard, J. Alloys Compd. 429 (2007) 192–197.
[23] J.M. Silveyra, M. Coisson, F. Celegato, P. Tiberto, F. Vinai, J.A. Moya, V.J. Cremaschi, J. Alloys Compd. 495 (2010) 412–416.
[24] A. Misra, J.P. Hirth, H. Kung, Philos. Mag. A 82 (2002) 2935–2951.
[25] F.J. Lamelas, C.H. Lee, H. He, W. Vavra, R. Clarke, Phys. Rev. B 40 (1989) 5837–5840.
[26] H.A.M. Degronckel, K. Kopinga, W.J.M. Dejonge, P. Panissod, J.P. Schille, F.J.A. Denbroeder, Phys. Rev. B 44 (1991) 9100–9103.
[27] W.C. Oliver, G.M. Pharr, J. Mater. Res. 7 (1992) 1564–1583.
[28] R. Saha, W.D. Nix, Acta Mater. 50 (2002) 23–38.
[29] D.L. Joslin, W.C. Oliver, J. Mater. Res. 5 (1990) 123–126.
[30] T.H. Courtney, Mechanical Behavior of Materials, China Machine Press, Beijing, 2004.
[31] M. Huang, P.E.J. Rivera-Diaz-del-Castillo, O. Bouaziz, S. van der Zwaag, Scripta Mater. 61 (2009) 1113–1116.
[32] J. Wang, R.G. Hoagland, A. Misra, Appl. Phys. Lett. 94 (2009) 131910.
[33] R. Roumina, B. Raeisinia, R. Mahmudi, Scripta Mater. 51 (2004) 497–502.
[34] O. Prakash, D.R.H. Jones, Acta Mater. 44 (1996) 891–897.
[35] P.M. Sargent, M.F. Ashby, Mater. Sci. Technol. Lond. 8 (1992) 594–601.
[36] M. Verdier, M. Fivel, B. Gilles, Adv. Eng. Mater. 3 (2001) 597–601.
[37] D. Mitlin, A. Misra, V. Radmilovic, M. Nastasi, R. Hoagland, D.J. Embury, J.P. Hirth, T.E. Mitchell, Philos. Mag. 84 (2004) 719–736.
[38] D. Mitlin, A. Misra, T.E. Mitchell, J.P. Hirth, R.G. Hoagland, Philos. Mag. 85 (2005) 3379–3392.
[39] F. Akasheh, H.M. Zbib, J.P. Hirth, R.G. Hoagland, A. Misra, J Appl. Phys. 102 (2007) 034314.
[40] J.G. Sevillano, I.O. Arizcorreta, L.P. Kubin, Mater. Sci. Eng. A 309 (2001) 393–405.
[41] J. Wang, R.G. Hoagland, A. Misra, Scripta Mater. 60 (2009) 1067–1072.